Journal of Visualization, Vol. 11, No. 3 (2008)221-229

Regular Paper

Performance of Synthetic Jet Actuators Based on Hybrid and Double-Acting Principles

Trávníček, Z.*, Tesař, V.* and Kordík, J.*

* Institute of Thermomechanics of the ASCR v. v. i., Dolejškova 5, 182 00 Prague, Czech Republic.
E-mail: tr@it.cas.cz

Received 22 October 2007
Revised 24 February 2008

Abstract : The design of the discussed fluid jet actuator followed two ideas: a double-acting operation of reciprocating pumps, and a hybrid synthetic jet (HSJ) actuation. The entire actuator consists of two basic parts, namely the front (central) and rear chambers, from which fluid is displaced by the opposite sides of the same diaphragm. The actuator operates in a double-acting (antiphase) regime with air as the working fluid. The central chamber generates the standard (zero-net-mass-flux) axisymmetric synthetic jet (SJ), while the rear chamber generates system of several non-zero-net-mass-flux HSJs arranged around the central SJ. A number of variants of HSJs with different geometry were designed, manufactured and tested. Their behavior was investigated experimentally using the smoke visualization, reaction force measurement, hot-wire anemometry, and naphthalene sublimation technique. The tests confirm the efficiency of the present design.

Keywords : Synthetic Jet, Impinging Jet, Actuator, Fluidic Diode, Heat Transfer, Visualization, Naphthalene Sublimation.

1. Introduction

Synthetic jets (SJs) are generated (synthesized) by the interactions within a train of vortices, created by an oscillatory process in fluid produced by pushing and pulling it periodically to and from a displacement cavity through an orifice (Smith and Glezer, 1998). A typical SJ actuator consists of the cavity bounded at one end by a wall with the exit orifice or nozzle, and at the other end by an actuating diaphragm or piston. The time-mean mass flow rate of the oscillatory flow in the orifice is zero, hence the other common expression is zero-net-mass-flux (ZNMF) jet (Cater and Soria, 2002).

The "hybrid synthetic jet" (HSJ) combines the ZNMF jet and a fluidic pumping by a valve-less pump – as described in previous publications by Trávníček et al. (2005a, 2005b and 2006), and Chen et al. (2006). In contrast to the standard SJ, the HSJ is an intrinsically non-zero-net-mass-flux jet. Despite no fluid being supplied from an external source (blower or compressor), HSJ exhibits a higher extrusion volume flow rate than the ordinary SJ. This increase is due to the fluidic rectification effect of the HSJ actuator (Trávníček et al., 2006).

It is worth noting here that another variant has been proposed by Tesař et al. (2005, 2006, and 2007) also named HSJ because it also generates non-ZNMF conditions in the orifice. It uses an actuator supplied by steady flow from an external source. The alternating flow there is generated by a fluidic (self-excited) oscillator, with the return flow produced by the jet-pumping effect. The volume flow rate is enhanced externally, i.e., independently of the oscillator function.

The *double-acting operation* is a well-known method, which is used in various devices such as reciprocating piston pumps and compressors. This method has been also applied to SJ actuator design: two actuator cavities separated by a common diaphragm, so that they operate in the antiphase – see, e.g., Lee and Goldstein (2002), Trávníček et al.(2004, 2005a and 2005b), and more recently Luo et al. (2006).

A submerged *impinging jet* (IJ) is the technique for achieving a very high intensity heat and mass transfer between fluid and walls. Continuous (steady) conventional IJs have been studied quite extensively during the last few decades (e.g., Martin, 1977; Dyban and Mazur, 1982; Downs and James, 1987; Jambunathan et al. 1992; Viskanta, 1993; Webb and Ma, 1995; Garimella, 2000).

SJs and HSJs offer many application possibilities in active control of flowfields and thermal fields, especially in external and internal aerodynamics, cooling of highly heated electronic components and turbine blades, drying technologies, mixing in chemical reactors, etc. The present paper focuses on the heat/mass transfer applications – see e.g., Trávníček and Tesař (2003), Kercher et al. (2003), Gillespie et al. (2006), and Arik (2006). The aim of the present study is to demonstrate novel variants of SJ actuators that offer distinct advantages to various heat/mass transfer applications. Also, we have aimed at quantifying some of their performance characteristics.

2. Experimental Setup and Methods

Figure 1 shows the design of the present double-acting actuator with trigonally arranged secondary (HSJ) nozzles. The entire actuator consists of two basic parts, namely the front and rear chambers (F and R), from which air is displaced by the opposite sides of the same diaphragm (2a). The standard SJ is generated from the front chamber F through its central round nozzle, and the rear chamber generates an array of three hybrid synthetic jets (HSJs) arranged trigonally around the central round SJ. Elements for inputting additional air consist of 12 identical radial conical ducts (4), equidistantly located on the chamber 1. The actuator operates in double acting regime, i.e., both the up- as well as the down- strokes of the diaphragm act on the displaced fluid. The positive stroke pushes fluid through the central circular nozzle creating the standard SJ, while the reverse one pushes fluid through the trigonal array of nozzles creating a non-ZNMF HSJs. The axisymmetric coordinate system (x, r) is also shown in Fig. 1.

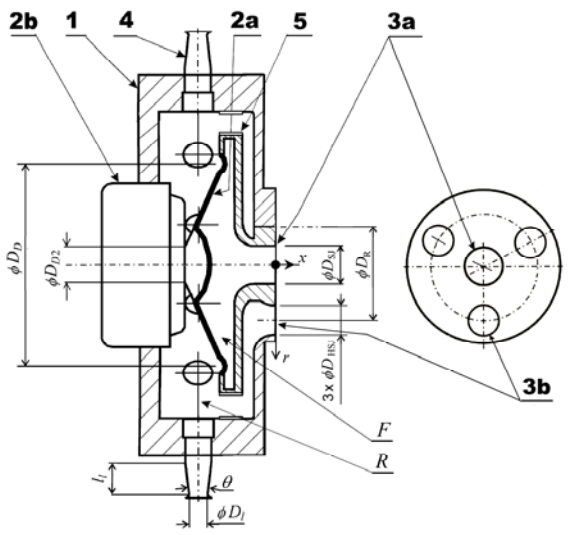

Fig. 1. Double-acting actuator with trigonally arranged HSJ nozzles, (a) cross-section and (b) side view on the trigonal arrangement of nozzles. F– front cavity, R– rear cavity, 1– chamber, 2a– diaphragm, 2b– drive unit (coil), 3a– central SJ nozzle, 3b– trigonal array of HSJ nozzles, 4– conical ducts (input element of the R-cavity), 5– fixed common interface; ϕD_{SJ} = 10.6 mm, ϕD_R = 28.5 mm, ϕD_{HSJ} = 8.0 mm, ϕD_D = 53.0 mm, ϕD_{D2} = 9.0 mm, ϕD_1 = 4.35 mm, l_1 = 8.0 mm, θ = 12.5°.

The described double acting principle is the same as the one used in the previous studies by Trávníček et al. (2005a and 2005b). However, the previously described actuator had a coaxial HSJ output while the present actuator generates an array of round HSJs. Air is moved by an electrodynamically driven diaphragm, originating from the loudspeaker (MONACOR SP-7/4S). The actuator is supplied with sinusoidal electric current at 2.0 W, which is the same as in the previous studies by Trávníček et al. (2005a and 2005b).

Second variant of the actuator tested in this study was equipped by six HSJs, hexagonally arranged around the central SJ: D_R = 25.0 mm and D_{HSJ} = 4.5 mm; other dimensions are the same as in Fig. 1.

An initial step in the experiments used the smoke-wire technique for flow visualization (Trávníček and Tesař, 2003). The phase-locked flow field pattern was observed under stroboscope light synchronized with the excitation frequency at an arbitrary phase angle, and pictures were taken by a digital camera.

A time-mean reaction force was measured similarly as in the previous paper by Trávníček et al., 2005a. The purposes were (1) demonstration of a properly functioning actuator, and (2) finding the "nominal actuating frequency", i.e., the frequency chosen for efficient actuation. This frequency was found as close to the resonance as possible (for the given geometry variant), and then it was adjusted to remain constant in all subsequent simultaneous measurements of velocity and mass transfer. A precision scale Mettler PR8002 with the resolution of 0.01g was used. Once the actuation begun, the time-mean reaction force was evaluated from the increase of the apparent nozzle weight. The maximum value at the resonance was 1.20–1.40 g, and the uncertainty of the time-mean reaction force at the resonance was estimated to be within 1 %.

Velocity distributions were measured using hot-wire anemometer DANTEC (MiniCTA 55T30) in the constant-temperature mode, with the single-sensor wire probe (55P16). Typical sampling frequency and number of samples were 15 kHz and 262 144, respectively. For the present experiments, the anemometer was calibrated in the velocity range from 0.8 to 40 m/s; the linearization error of the calibration (using a fifth-degree polynomial) was within 3 %, and the velocity sample uncertainty was estimated to be within 6 %. The phase averaging of the velocity during one cycle was carried out using velocity decomposition $u = U + U_f + u'$, where U is the time-mean velocity, U_f is the periodic phase-locked component, and u' is the fluctuating component. Taking into account the pulsating velocity character in the actuator orifice, positive (extrusion) and negative (suction) flow orientations (indistinguishable by the single-wire probe) were obtained by inverting appropriately the velocity sign during the suction stroke.

Local mass transfer in impinging jet flows was measured using the naphthalene sublimation method (Trávníček and Tesař, 2003; Goldstein and Cho, 1995). The non-dimensional expression of the mass transfer coefficient is the Sherwood number, defined as $Sh = h_m D_{SJ}/D_n$, where h_m is the local mass transfer coefficient, D_{SJ} is the central SJ nozzle diameter (Fig. 1), and D_n is the mass diffusion coefficient of naphthalene vapor in air, calculated for measured temperature and pressure conditions. The mass-transfer result was recalculated following the heat/mass transfer analogy $Nu/Pr^{0.4} = Sh/Sc^{0.4}$ to predict the heat transfer distribution, where Nu, Pr and Sc are the Nusselt, Prandtl, and Schmidt numbers, respectively (Goldstein and Cho, 1995). The uncertainty of the mass transfer coefficient and the Sherwood number is within 6 % and 9 % ; a more detailed description of the experimental method and uncertainties is available in Trávníček and Tesař (2003).

3. Results and Discussions

Figure 2 shows the frequency characteristics in form of the measured time-mean reaction force for three different variants of the HSJ outputs: the coaxial output from the previous experiment by Trávníček et al. (2005a), and the present trigonal and hexagonal arrangements of the HSJs. The parameter a of the HSJ is defined as the ratio of the cross-sectional areas in the throats of the input conical ducts and the cross-sectional areas of output HSJ nozzles. Figure 2 shows that increasing a-value results in the increase of the reaction force of the actuator with the coaxial HSJ (Trávníček et al., 2005a); the increase becomes nearly saturated for a = 1.158–1.737. Based on this experience, the

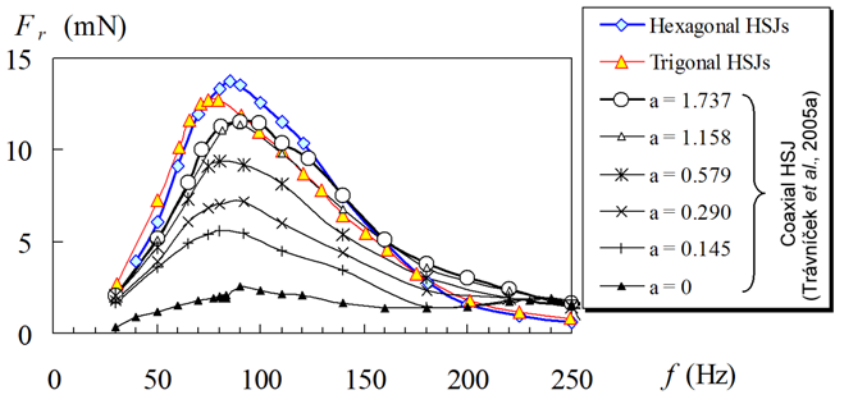

Fig. 2. Frequency characteristics of three variants of the HSJ outputs – time-mean reaction force.

present actuators were design with quite high a- values in an attempt to obtain their high performance: a = 1.18 and 1.87 for the trigonal and hexagonal HSJs, respectively.

Figure 2 shows that the reaction force of both present actuators is higher than in the previous variant with the coaxial HSJ. The highest value is achieved with the hexagonal HSJs. The maximum reaction force of the present actuators is achieved for frequencies f = 75–85 Hz, hence both present actuators with trigonal and hexagonal HSJs were tested at f = 80 Hz.

To illustrate the jet formation process at the trigonal arrangement of HSJs, Fig. 3 shows the phase-locked presentation during the actuating period. Figures 3(a) and 3(b) were made by means of the smoke-wire visualization and hot-wire measurement, respectively. Figure 3(a) shows the phase-locked visualization for 8 equal time intervals during the period; the images were made as the multi-exposure of 80 stroboscope flashes. For better illustration, the time period of the actuation signal was chosen to be represented by 360 angular degrees. Therefore, the phase angle φ (from 0° to 360°) is used as the measure of the dimensionless time in the cycle t/T (from 0 to 1). The period origin (φ = 0°) is defined by the start of the central SJ extrusion stroke (i.e., when the instantaneous velocity in the SJ nozzle is zero and the deflection of the diaphragm from its neutral position is maximum). The entire cycle of the central SJ consists of the extrusion and suction strokes, which are during phase angles φ = 0°–180° and 180°–360°, respectively. In the same strokes, the HSJ actuator operates with opposing phases at the suction and extrusion strokes, respectively.

The orientation of the extrusion/suction velocity of the central SJ is indicated by the arrows at the left hand side of the photographs in Fig. 3(a). The main feature, visible in the sequence of photographs, is the generated fluid "puff", i.e., the large vortex structure passing downstream across the observation area. The location of the structure agrees very well with the hot-wire measurement result, namely with the maximum of the traveling wave on the instantaneous velocity curve (red line in Fig. 3(b)).

The extrusion of fluid through the central SJ orifice and the formation of the large vortex structure near the orifice is well visible at φ = 30°–165° in Fig. 3(a). At the same time, fluid is ingested by the trigonal array of HSJs. The main proportion of this fluid comes from the relatively quiescent surroundings, and only a small portion is taken from the just extruded central puff. Because of the arrangement of the HSJs is trigonal, the flow pattern in the observation plane seems to be non-symmetrical.

Later, at φ = 210°–345°, the central SJ actuator operates in the suction stroke ingesting the external fluid. However, the inertia of the large vortex structure results in its moving downstream irrespective of the local situation in the nozzle, where the flow orientation is reversed. At the same time, the trigonal array of HSJs pushes fluid outwards from the actuator, as is well visible at φ = 345°. This HSJs outflow partially promoted the entire jet formation, and partially is reversed inwards into the central SJ – which is in the suction stroke.

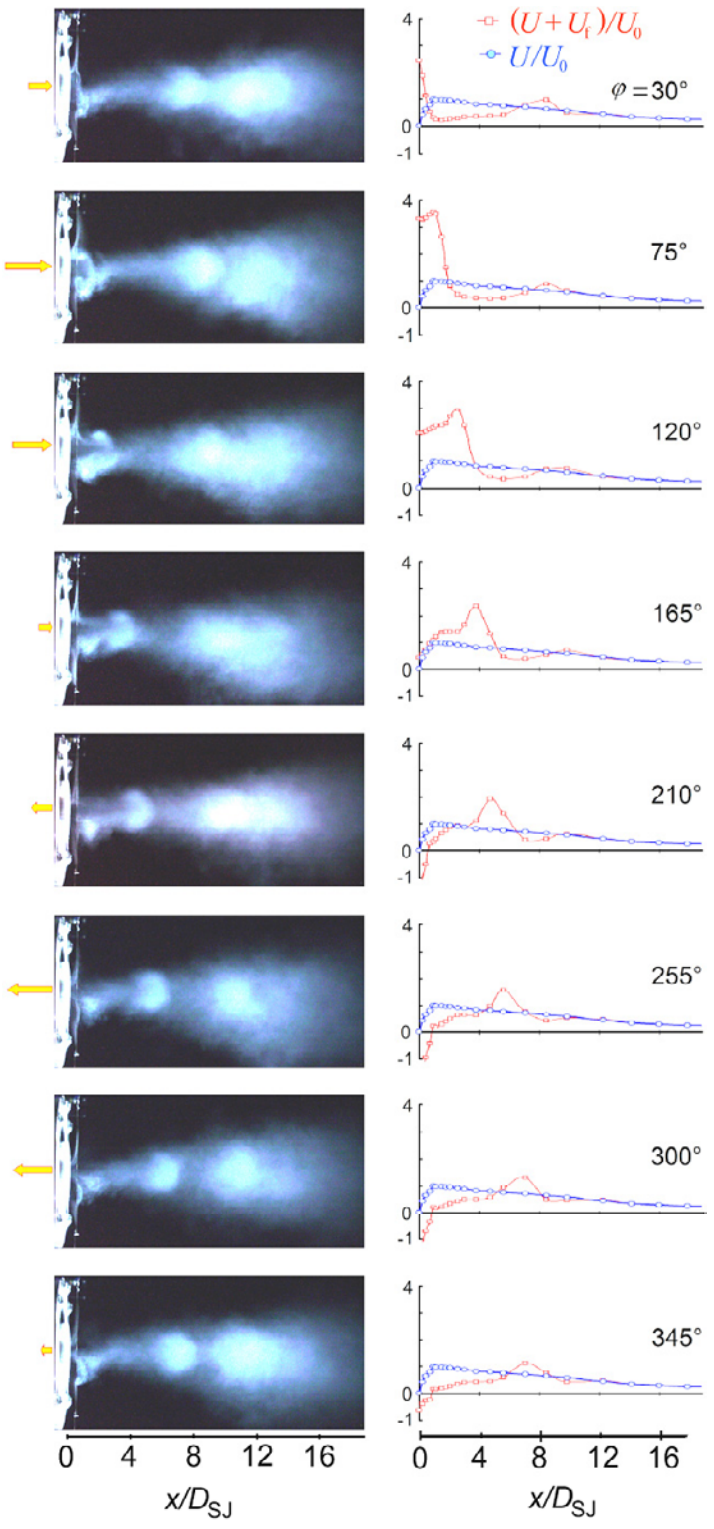

Fig. 3. Phase-locked presentation of the period for trigonally arranged HSJs; (a) smoke visualization, (b) hot-wire measurement (the red line with square symbols denotes the instantaneous velocity, the blue line with circles denotes the time-mean velocity).

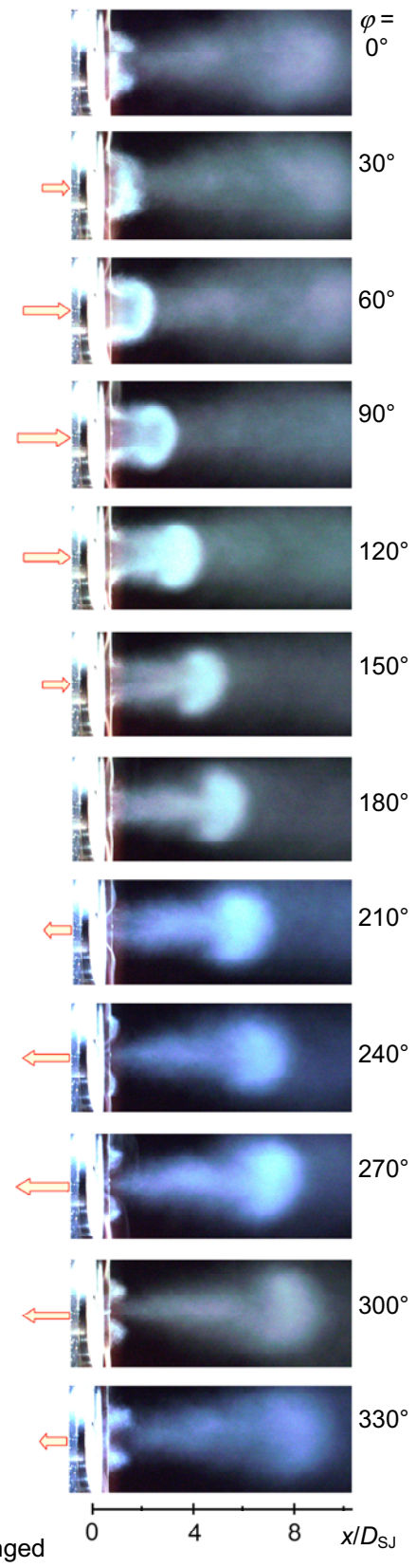

Fig. 4. Phase-locked visualization of the period of the actuator with hexagonally arranged HSJs.

However, the ingestion range of the actuator is relatively small, up to $x/D_{SJ} = 0.85$ – see the hot-wire measurement in Fig. 3(b) at $\varphi = 300°–345°$. For $x/D_{SJ} > 0.85$, the inertia of the large vortex structure results always in moving downstream independently of the local situation in the orifice. Finally, at $\varphi = 360°$ (i.e., $t/T = 1$), the whole cycle is repeated.

Figure 4 shows the similar visualization at the hexagonal arrangement of HSJs for 12 equal time intervals during the period. Instead of the trigonal variant in Fig. 3(a), the hexagonal geometry of HSJs results in obvious symmetry in each moment. Note that this hexagonal arrangement is promising because it causes the highest maximum reaction force – see Fig. 2 above.

Figure 5 compares the phase-averaged velocity cycles of the central SJ, trigonally arranged HSJs, and input conical ducts (position 4 in Fig. 1), which were measured on their axes, at the actuator exit. The positive and negative sign of the velocities mean the extrusion and suction, respectively.

To show the absolute differences between them, the diagrams are plotted in the dimensional form. The velocity cycle of the central SJ is approximately four times larger than of trigonal HSJs and the input conical ducts. The time-mean nozzle velocity is defined from the nozzle velocity on the axis $u_0(t)$ as $U_0 = f \int_0^{T_E} u_0(t)\,dt$, where t is time, T_E is the extrusion time, and f is the actuation frequency. This definition is slightly modified in comparison with a common definition by Smith and Glezer (1998) taking into account the fact that the extrusion time may be different (namely for our actuators) from the half-period, $T_E \neq T/2$.

The integration of curves from Fig. 5 over the extrusion stroke gives the time-mean orifice velocities of the central SJ, trigonal HSJs, and input conical ducts $U_0 = 6.07$ m/s, 1.70 m/s and 1.51 m/s, respectively. The corresponding Reynolds numbers, defined from the mentioned velocities and the corresponding diameters D_{SJ}, D_{HSJ} and D_1 are $Re_0 = 3970$, 840 and 400, respectively.

The stroke lengths, $L_0 = U_0\ T$, of the central SJ, trigonal HSJs, and input conical ducts are 7.18 D_{SJ}, 2.68 D_{HSJ}, and 4.37 D_1, respectively; T is the time period $T = 1/f$.

The non-symmetry of the pump and supply strokes of the trigonal HSJs in Fig. 5 demonstrates the fluidic *rectification effect* of the input conical ducts (position 4 in Fig. 1). The performance criterion is the *volumetric efficiency* ε_V, defined as the ratio of the net output fluid volume during the entire period to the total fluid volume pumped during the same time (Trávníček et al., 2006). While all ZNMF actuators exhibit $(\varepsilon_V)_{SJ} = 0$, the HSJs yields $(\varepsilon_V)_{HSJ} > 0$. The true $(\varepsilon_V)_{HSJ}$ value has to be evaluated from the average velocity across the cross sections, but it was not measured in this study. Therefore, $(\varepsilon_V)_{HSJ}$ value was estimated from the pump and supply strokes of the trigonal HSJs in Fig. 5. The integration of velocity cycle gives 24 %. Taking into account the previous results of the velocity profiles in SJ actuator orifices (Trávníček et al., 2006), the integration result was corrected to $(\varepsilon_V)_{HSJ}$ = 19 %. This result agrees reasonably with the conclusion of HSJ measurement by Trávníček et al. (2006), where a similar conical duct has led to $(\varepsilon_V)_{HSJ}$ = 23 %.

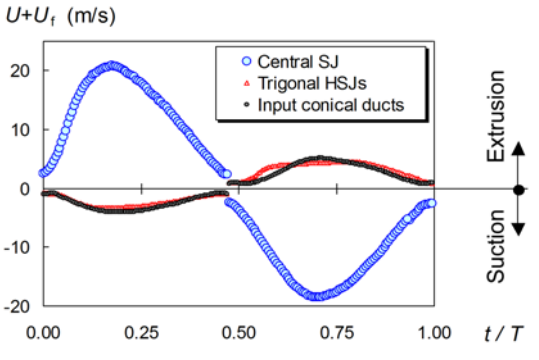

Fig. 5. Phase-averaged velocity cycles of the central SJ, trigonally arranged HSJs, and input conical ducts.

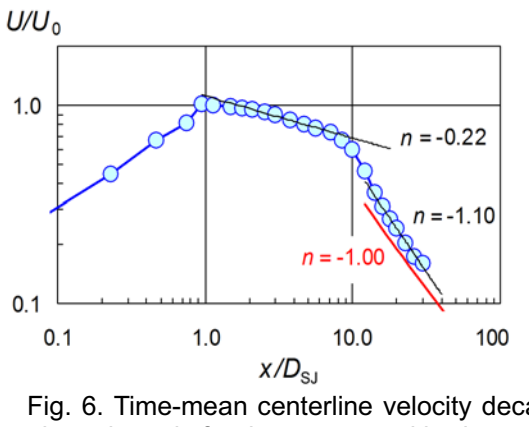

Fig. 6. Time-mean centerline velocity decay along the axis for the actuator with trigonally arranged HSJs.

Figure 6 shows the streamwise variation of the time-mean velocity along the jet centerline, plotted in logarithmic scales. First, the time-mean velocity gradually increases with distance from the actuator – the jet is synthesized. The maximum time–mean velocity is approximately $1.0\,U_0$ at $x/D_{SJ} = 1.0$. Further downstream, the time–mean velocity decreases. Two distinguishable ranges can be quantified according to the proportionality $U/U_0 \sim (x/D_{SJ})^n$: At the beginning, $x/D_{SJ} = 1.5$–8.5, the velocity decreases by the exponent n = –0.22. At a location more downstream, the slope is steeper with n = –1.10 for $x/D_{SJ} = 14$–30. Quite similar behavior was described previously for the actuator with the coaxial HSJ output (Trávníček et al., 2005b). Moreover, the streamwise time–mean velocity decay at a location more downstream approximately agrees with the well known behavior of the conventional (steady) axisymmetric fully developed turbulent jets with the decay $U \sim x/D^{-1.0}$ (Schlichting, 1979).

Figure 7 presents examples of the local heat/mass transfer at nozzle-to-wall distances H/D_{SJ} = 2, 6, 10 and 16 for the present double-acting actuator with hexagonally arranged HSJs. Because of the satisfactory symmetry, the curves were evaluated by averaging the two halves of each experimental profile. The highest values occurred always in the stagnation point on the axis. The local Nusselt number decreases monotonously with the radial distance from the stagnation point creating bell-shaped distributions. The "secondary peaks" of the heat transfer distribution did not occur, although they are usually significant for IJs at small nozzle-to-wall distances $H/D_{SJ} = 2$. In fact, this absence reasonably agrees with the literature – it is known that the secondary peaks are significantly reduced or even suppressed by turbulence promotion and periodic excitations (e.g., Garimella, 2000).

Figure 8 shows the variation of the stagnation point heat/mass transfer with the nozzle-to-wall spacing H/D_{SJ}. The present data are compared with those obtained using the representative correlations of continuous IJs for the same $H/D = 2$–16 at $Re = 3970$ (Popiel and Boguslavski, 1986; Garimella and Rice, 1995). Figure 8 shows that the present results correspond well to the heat/mass transfer of the steady IJs. On the other hand, the effect of the nozzle-to-wall spacing at small distances seems to be different from that of the continuous IJ: While the maximum Nu_0 is achieved around $H = 5D$ for the continuous IJs, the decrease of the spacing from $H = 5D_{SJ}$ to $2D_{SJ}$ for the present actuator causes monotonous increase of the Nu_0. It can indicate a promising benefit of the actuator primarily at very small nozzle-to-wall spacings.

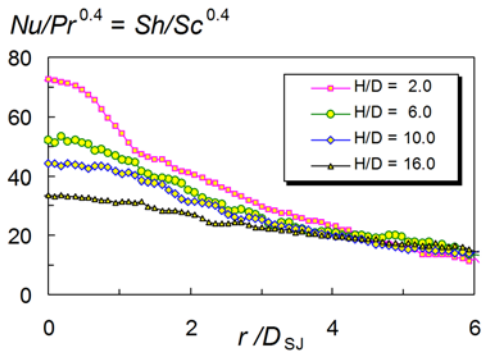

Fig. 7. Local heat/mass transfer onto impingement wall for the actuator with hexagonally arranged HSJs.

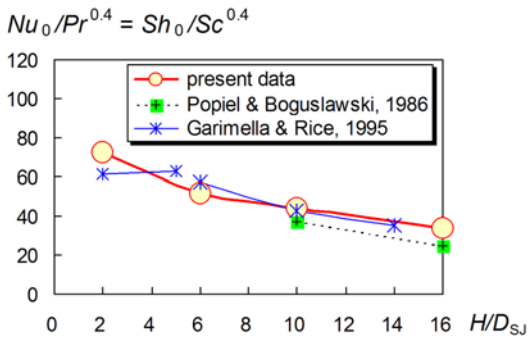

Fig. 8. Stagnation point heat/mass transfer: comparison of the present experiments for hexagonally arranged HSJs with representative correlations for continuous IJs.

4. Conclusions

A very compact, double-acting actuator actuator for generation of hybrid synthetic jets (HSJ) was developed. It generates a system of air jets: the central round (classical) synthetic jet and an array of three or six HSJs arranged trigonally or hexagonally around the central jet. A behavior of the flowfield was investigated experimentally using the smoke visualization, reaction force measurement, hot-wire anemometry and naphthalene sublimation technique.

The volumetric efficiency of the present HSJ was evaluated to be approximately $(\varepsilon_V)_{HSJ} = 19$ %, while the synthetic jets exhibit always $(\varepsilon_V)_{SJ} = 0$. The stagnation point heat/mass transfer of the present jet corresponds well to the heat/mass transfer of the continuous impinging jets. Moreover, the present jet gives slightly higher stagnation heat/mass transfer at the smallest nozzle-to-wall spacings.

Acknowledgements

We gratefully acknowledge the support of the GACR (101/07/1499), GAASCR (IAA200760801), and research project AV0Z20760514.

References

Arik, M., An investigation into feasibility of impingement heat transfer and acoustic abatement of meso scale synthetic jets, Applied Thermal Engineering, 27 (2007), 1483-1494.
Cater, J. E. and Soria, J., The evolution of round zero-net-mass-flux jets. J. Fluid Mech., 472 (2002), 167-200.
Chen, C-C., Chou, C-C., Hsu, S-S. and Wang, A-B., Visualization of new synthetic jet actuator for underwater vehicles, Proceedings of the 12th International Symposium on Flow Visualization (ISFV-12)(Göttingen), 86.4 (2006).
Downs, S. J. and James, E. H., Jet impingement heat transfer – a literature survey, Proceedings of the National Heat Transfer Conference, ASME (Pennsylvania), (1987), 87-HT-35.
Dyban, E. P. and Mazur, A. I., Convection Heat Transfer in Impinging Jets (Konvektivnyj teploobmen pri strujnom obtekanii tel), 1st ed., Naukova dumka, Kiev, (1982) (in Russian).
Garimella, S. V., Heat transfer and flow fields in confined jet impingement, Annual Review of Heat Transfer, XI, 413 (2000), 413-494.
Garimella, S. V. and Rice, R. A., Confined and submerged liquid jet impingement heat transfer. Trans. ASME J. Heat Transfer, 117 (1995), 871-877.
Gillespie, M. B., Black, W. Z., Rinehart, C. and Glezer, A. Local convective heat transfer from a constant heat flux flat plate cooled by synthetic air jets. Trans. ASME, J. Heat Transfer, 128 (2006), 990-1000.
Goldstein, R. J. and Cho, H. H., A review of mass transfer measurements using naphthalene sublimation. Exp. Thermal Fluid Sci., 10 (1995), 416-434.
Jambunathan, K., Lai, E., Moss M. A. and Button B. L., A review of heat transfer data for single circular jet impingement, Int. J. Heat Fluid Flow, 13-2 (1992), 106-115.
Kercher, D. S., Lee, J.-B., Brand, O., Allen, M. G. and Glezer, A., Microjet cooling devices for thermal management of electronics, IEEE Transactions on Components and Packaging Technologies, 26-2 (2003), 359-366.
Lee, C. Y. and Goldstein, D. B., Simulation of MEMS suction and blowing devices for turbulent boundary layer control. In: 1st Flow Control Conference (St. Luis, Missouri, USA), AIAA 2002-2831, (2002-6).
Luo, Z-B., Xia, Z-X. and Liu, B., New generation of synthetic jet actuators. AIAA J., 44-10 (2006), 2418-2420.
Martin H., Heat and mass transfer between impinging gas jets and solid surfaces, Adv. Heat Transfer, 13 (1977), 1-60.
Popiel, C. O. and Boguslavski, L., Mass or heat transfer in impinging single, round jets emitted by a bell-shaped nozzle and sharp-ended orifice. Proc. 8th Int. Heat Transfer Conference (San Francisco, USA), 3 (1986), 1187-1192.
Schlichting, H., Boundary Layer Theory, 7th ed. (1979), McGraw-Hill, New York.
Smith, B. L. and Glezer, A., The formation and evolution of synthetic jets, Phys. Fluids, 10 (1998), 2281-2297.
Tesař, V., Hung C-H. and Zimmerman, W. B., No-moving-part hybrid-synthetic jet actuator, Sensors and Actuators A, 125-2 (2006), 159-169.
Tesař, V. and Trávníček, Z., Pulsating and synthetic impinging jets. Journal of Visualization, 8-3 (2005), 201-208.
Tesař, V. Trávníček, Z., Kordík, J. and Randa, Z., Experimental investigation of a fluidic actuator generating hybrid-synthetic jets. Sensors and Actuators A, 138 (2007), 213-220.
Trávníček, Z., Fedorchenko, A. I. and Wang A-B., An enhancement of synthetic jets by means of an integrated valveless pump. In: Proceedings of the Tenth Asian Congress of Fluid Mechanics (Peradeniya, Sri Lanka), (2004-5), 535-540.
Trávníček, Z., Fedorchenko, A. I. and Wang, A-B., Enhancement of synthetic jets by means of an integrated valve-less pump, Part I: Design of the actuator. Sensors and Actuators A, 120-1 (2005a), 232-240.
Trávníček, Z., Tesař, V. and Wang, A-B., Enhancement of synthetic jets by means of an integrated valve-less pump, Part II: Numerical and experimental studies, Sensors and Actuators A, 125-1 (2005b), 50-58.
Trávníček, Z., Vít, T. and Tesař, V., Hybrid synthetic jet as the non-zero-net-mass-flux jet. Phys. Fluids, 18-8 (2006), 081701-1-081701-4.
Trávníček, Z. and Tesař, V., Annular synthetic jet used for impinging flow mass–transfer, Int. J. Heat Mass Transfer, 46 (2003), 3291-3297.
Viskanta, R., Heat transfer to impinging isothermal gas and flame jets, Exp. Therm. Fluid Sci., 6 (1993), 111-134.
Webb, B. W. and Ma, C.-F., Single-phase liquid jet impingement heat transfer, Adv. Heat Transfer, 26 (1995), 105-107.

Authors Profiles

Zdeněk Trávníček: He received his M.Sc. (Eng.) degree in Mechanical Engineering from the Czech Technical University (CTU) in Prague in 1985 and his Ph.D. from the same university in 1994. From 1985 to 1995, he was employed at the former National Research Institute for Machine Design (SVÚSS) in Prague Běchovice. In 1996, he joined the Institute of Thermomechanics, Academy of Sciences of the Czech Republic. Since 2004, he is the Head of the Heat/Mass Transfer Laboratory. His research interests cover experimental fluid mechanics and heat/mass transfer, passive/active thermal flow control (primarily of jets and wakes), forced convective heat/mass transfer enhancement, and impinging and synthetic jets.

Václav Tesař: He received his degree in mechanical engineering and later CSc degree (an equivalent of PhD) from CTU Prague. He was Head of the Department of Fluid Mechanics and Thermodynamics, Faculty of Mechanical Engineering CTU Prague. In 1985, he was Visiting Professor at Keio University, Yokohama, Japan and in 1992 a Visiting Professor at Northern Illinois University, DeKalb, USA. Between 1999 and 2005 he was Professor at the Department of Chemical and Process Engineering, the University of Sheffield, UK. In 2006 he joined the Institute of Thermomechanics, Academy of Sciences of the Czech Republic. His research interests are in shear flows - in particular jets and wall jets - and their applications in fluidics.

Jozef Kordík: He received his M.Sc. (Eng.) degree in Mechanical Engineering from the Czech Technical University (CTU) in Prague in 2007. From 2006 has been employed on part-time basis at the Institute of Thermomechanics, Academy of Sciences of the Czech Republic. Since 2007, he is the Ph.D. student at the CTU. His interest and subject of his Ph.D. studies are experimental investigations of unsteady flows and computer processing of complex experimental data sets.